Published in final edited form as:
Anal Chem. 2013 October 1; 85(19): . doi:10.1021/ac402262e.

Single Cell Metabolic Profiling of Tumor Mimics

Richard B. Keithley[†], **Eric M. Weaver**, **Andrea M. Rosado**, **Mark P. Metzinger**, **Amanda B. Hummon**, and **Norman J. Dovichi**[*]
Department of Chemistry and Biochemistry, University of Notre Dame, Notre Dame, IN 46556, USA

Abstract

Chemical cytometry employs modern analytical methods to study the differences in composition between single cells to better understand development, cellular differentiation, and disease. Metabolic cytometry is a form of chemical cytometry wherein cells are incubated with and allowed to metabolize fluorescently labeled small molecules. Capillary electrophoresis with laser-induced fluorescence detection is then used to characterize the extent of metabolism at the single cell level. To date, all metabolic cytometry experiments have used conventional two-dimensional cell cultures. HCT 116 spheroids are a three-dimensional cell culture system, morphologically and phenotypically similar to tumors. Here, intact HCT 116 multicellular spheroids were simultaneously incubated with three fluorescently labeled glycosphingolipid substrates, GM3-BODIPY-FL, GM1-BODIPY-TMR, and lactosylceramide-BODIPY-650/665. These substrates are spectrally distinct, and their use allows the simultaneous probing of metabolism at three different points in the glycolipid metabolic cascade. Beginning with intact spheroids, a serial trypsinization and trituration procedure was used to isolate single cells from spatially distinct regions of the spheroid. Cells from the distinct regions showed unique metabolic patterns. Treatment with the lysosomal inhibitor and potential chemotherapeutic chloroquine consistently decreased catabolism for all substrates. Nearly 200 cells were taken for analysis. Principal component analysis with a multivariate measure of precision was used to quantify cell-to-cell variability in glycosphingolipid metabolism as a function of cellular localization and chloroquine treatment. While cells from different regions exhibited differences in metabolism, the heterogeneity in metabolism did not differ significantly across the experimental conditions.

Three-dimensional cell culture is a relatively new *in vitro* system that recapitulates portions of the *in vivo* environment while retaining the benefits of traditional cell and tissue culture.[1] For some cell types, three-dimensional cell culture can produce a multi-cellular tumor spheroid (MCTS) architecture. Like cells in tissue, cells in MCTS adopt polarity that can produce distinct spheroid microenvironments.[2,3]

As tumors develop *in vivo*cellular areas distal to blood vessels are deprived of nutrients and oxygen and cannot remove waste products from adjacent cells; nutrient depravation leads to formation of hypoxic and necrotic areas.[3–4] Conversely, the parts of the tumor that are proximal to blood vessels are well-oxygenated and exposed to a variety of different growth factors secreted by neighboring cells; these nutrient rich regions are highly active and proliferative.

[*]To whom correspondence should be addressed. Fax: 574-631-6652; Tel: 574-631-2778; Norman.J.Dovichi.1@nd.edu.
[†]Current Address: Department of Chemistry, Roanoke College, Salem, VA 24153

SUPPORTING INFORMATION
Supporting Information Available: This material is available free of charge via the Internet at http://pubs.acs.org.

Three-dimensional cell culture mimics these gradients *in vitro*. Under proper conditions, HCT 116 colon carcinoma cells can aggregate into a single MCTS that reach up to 1 mm in diameter.[5] As the MCTS grow, the cells near the center become nutrient starved and ultimately die as the surrounding cells restrict access to the growth media. The cells on the outside of the spheroids remain metabolically active and proliferative.[6] The cells in the middle layers lapse into a quiescent state where they are metabolically active but not proliferating. Areas of necrosis and apoptosis increase with time, producing a central mass of cell debris surrounded by a layer of nutrient-starved but still living cells that are likely in a pre-necrotic state.[7] Serial trypsinization is a well-established technique to probe the microenvironments of MCTS.[8–11] Dilute trypsin is used to gently peel intact layers of cells from the outer regions spheroids. The process is repeated until the necrotic core containing only dead cells and cellular debris is reached.

Metabolic cytometry combines capillary electrophoresis with laser-induced fluorescence detection (CE-LIF) to probe metabolism in single cells.[12] In this approach, cells are incubated with a fluorescently labeled substrate. Single cells are then aspirated into a capillary and lysed. The fluorescent metabolites are separated and detected with CE-LIF.

In this paper, we use metabolic cytometry to investigate the metabolism of glycosphingolipids (GSLs) in different regions within MCTSs. GSLs constitute 5 - 20% of cell surface lipids, depending on the cell type.[13] GSLs are involved in a variety of cellular processes, and defects in their metabolism are associated with a number of diseases, including cancer.[14–16] These amphiphilic molecules consist of a nonpolar ceramide lipid tail and a polysaccharide headgroup. Figure S-1 (Supporting Information) presents simplified overview of GSL metabolism in colon carcinomas.[17–19] Synthetic GSLs have been prepared with fluorophores attached to the ceramide tail for use as substrates in metabolic cytometry studies of several systems.[20–29]

There is interest in using drugs to perturb metabolism in chemical cytometry. Chloroquine, an anti-malarial,[30] inhibits catabolism in several ways. Equilibrative transport brings it to the lysosome where it increases the intralysosomal pH from 4.7 to 6.2.[31] Chloroquine targets several lysosomal hydrolases.[32] Chloroquine effects catabolism on a transport level, inhibiting cell membrane recycling[33] and endosomal fusion with the lysosome.[34] Finally, chloroquine also acts an autophagy inhibitor and a novel potential chemotherapeutic.[35–36]

EXPERIMENTAL SECTION

Chemicals and Reagents

TRIS buffer, sodium dodecylsulfate, agarose, ethanol, and chloroquine (diphosphate salt) were from Sigma Aldrich. CHES buffer, α-cyclodextrin, and paraformaldehyde were from Alfa Aesar. Glycine was from VWR. HCT 116 cells were obtained from American Type Cell Culture. Phosphate-buffered saline (PBS), trypsin, McCoy's 5A cell culture media, and L-glutamine were from Life Technologies. Fetal bovine serum was from ThermoFisher. All buffers and stock solutions were prepared using distilled deionized water. GM3-BODIPY-FL, GM1-BODIPY-TMR, and LacCer-BODIPY-650/665 were kind gifts from Ole Hindgaul and Monica Palcic, synthesized as described previously.[21–22]

HCT 116 MCTS Culture and Lipid Incubation

Aliquots of 6 nmol each from stock solutions of GM3-BODIPY-FL (in dH_2O), GM1-BODIPY-TMR (in dH_2O), and LacCer-BODIPY-650/665 (in ethanol) were combined with 9 nmol methyl-β-cyclodextrin (in dH_2O) and dried using a Savant SpeedVac. Methyl-β-cyclodextrin acts as a lipid carrier, increasing cellular uptake of the fluorescent GSLs.[25]

Approximately 75 nmol of chloroquine (in dH_2O) was added to another set of 6 nmol each fluorescent GSLs and this solution was also dried using the SpeedVac.

Three-dimensional HCT 116 MCTSs were cultured in McCoy's 5A culture medium supplemented with 10% fetal bovine serum and 2.5 mM L-glutamine.[5] Approximately 6000 cells were seeded into each of 30 wells of a 96 well plate, resting on an agarose meniscus. After 14 days in culture, the cells formed uniform spheres of ~1 mm diameter in the center of each well.

On the day of MCTS incubation, aliquots of lipids with and without chloroquine were each resolubilized in 15 μL ethanol and diluted to a final volume of 3 mL with culture medium containing only 5% fetal bovine serum. This dilution yielded final concentrations of 2 μM for each of the fluorescent lipids and 25 μM chloroquine. When incubating with fluorescent GSLs, the lipids can preferentially partition into serum proteins rather than cellular surfaces; either reduced-serum or serum-free medium have been used to enhance uptake.[37] The cell culture medium used to grow the HCT 116 MCTSs was removed and replaced with either 200 μL of reduced-serum cell culture medium containing the fluorescent GSLs or 200 μL of reduced-serum cell culture medium containing the fluorescent GSLs and chloroquine. Thirty spheroids were treated with fluorescent GSLs for 24 hours. Half were treated with fluorescent GSLs alone and half with GSLs plus chloroquine. After incubation, the spheroids were removed from the 96-well plate and washed with serum-free medium to remove excess GSLs, chloroquine, and serum prior to serial trypsinization and single cell isolation.

Single Cell Isolation

Figure 1 presents an overview of the experiment. Fifteen spheroids treated only with the fluorescent GSL substrates were subjected to serial trypsinization.[8] The spheroids were incubated with chilled 0.05% trypsin/EDTA for 3 min at room temperature with gentle agitation to dislodge intact cellular layers. After 3 min, chilled media with serum was added to quench proteolysis. The wash medium was collected containing a grouping of cellular layers. The serum-free medium washing, trypsinization, and serum-containing medium washing steps were repeated. Layers from the first three treatments were pooled and labeled as the outer surface of the spheroids (Figure 2 - orange, referred to as outer). Cell layers from three subsequent treatments (fractions 4–6) were pooled representing an intermediate quiescent middle region of the spheroids (magenta, labeled as middle). The dead cells and necrotic cell debris (grey) were discarded, and the remaining cells, representing pre-necrotic cells (cyan, labeled as core) were selected as the third group. Each of these populations of intact cells was washed three times with PBS. Each group of cells was triturated by rapidly pipetting the solution to produce a single cell suspension. Approximately 1/3 of the suspensions were each incubated with 4% paraformaldehyde in PBS to fix cells; the other 2/3 were homogenized and stored at −80 °C. Fixing was halted using a wash of 10 mM glycine in PBS followed by two additional washes of PBS. Single cells were then resuspended in PBS and stored at 4 °C until analysis. The procedure carried out in parallel for fifteen spheroids incubated with fluorescent GSLs and chloroquine.

CE-LIF

The three-color single-cell CE system has been described elsewhere.[22] Solid-state lasers produced excitation at 473, 532, and 633 nm. Detection used a sheath-flow cuvette.[38] The red, green, and blue laser beams were focused ~50 μm, 70 μm, and 90 μm downstream from the capillary terminus, respectively, to minimize photobleaching and spectral crosstalk.[2229] Fluorescence was detected in three spectral channels with single-photon counting avalanche photodiodes.

The separation buffer was 100 mM TRIS, 100 mM CHES, 20 mM sodium dodecylsulfate, and 5 mM α-cyclodextrin. 30-μm ID, 150-μm OD, 50–55 cm long uncoated fused silica capillary (Polymicro) were used for the separation. A Spellman CZE1000R high voltage power supply was used to drive the separation at 26 kV. A locally constructed Plexiglas injection assembly was used to introduce running buffer and single cells onto the capillary.[27]

An Olympus IX70 inverted microscope was used for cell injection.[27] A 5 μL suspension of cells in PBS was placed onto a glass slide. The separation capillary, held in the injection assembly, was lowered with a micromanipulator until the capillary was a few micrometers above a cell of interest. A two-second pulse of negative pressure (11 kPa) injected a cell into the capillary. The capillary inlet was then placed in a solution of running buffer, and cells were incubated within the capillary for two minutes before the separation voltage was applied. A total of 212 cells were analyzed over a 30 day period after fixing. A new capillary was used at the beginning of each day and cells from the six conditions (outer, middle, and core, with/without chloroquine) were sampled randomly. Cell diameters were measured using the inverted microscope equipped with a 2.0 megapixel camera, and accompanying software (Motic Group). The cells used for diameter measurements were from the same six subpopulations as those analyzed by CE-LIF, but were not the same cells that were electrophoresed.

A handful of cells were analyzed using 10 mW laser power, which sometimes resulted in a fluorescence signal that saturated the photodetectors. Out of the total 212 cells analyzed, data from 20 cells were discarded because of saturation, poor signal-to-noise ratios, poor peak resolution or shape, and traces that could not be properly aligned. A total of 192 single cell multicolor electropherograms were processed further.

Data Analysis

Data analysis was performed in MATLAB. Electropherograms were corrected for dead time of the avalanche photodiode[39–40], treated with a five-point median filter to remove spikes, and smoothed by convolution with a 0.1 s wide Gaussian filter function. A two-point algorithm was used to temporally align the electropherograms based on the migration of GM1-BODIPY-TMR and Cer-BODIPY-TMR.

BODIPY-FL generated a small amount of spectral crosstalk into the BODIPY-TMR channel (<1.5%); the BODIPY-TMR labeled GSLs exhibited less spectral crosstalk into the BODIPY-650/665 channel (~ 0.1%). Spectral crosstalk was removed by subtraction.

Peak identities were based on the known migration pattern of BODIPY-labeled GSLs.[21–22] Peak areas were estimated by fitting each peak with a Gaussian function. The overlapping GlcCer and Cer peaks were fit with the sum of two Gaussian functions. To correct for differences in cellular uptake and laser powers, each electropherogram was normalized by the total fluorescence peak area in each spectral channel.

All reported uncertainties are the standard error of the mean.

Principal component analysis was performed by first trimming each electropherogram to isolate the separation window (9 – 10.3 minutes). The three-color traces from each cell were then concatenated into a single vector. The BODIPY-TMR data was appended after the BODIPY-FL data followed by the BODIPY-650/665 data. The data were mean-centered by subtracting the average concatenated electropherogram from all electropherograms. Principal component analysis was performed using singular value decomposition.[41]

RESULTS AND DISCUSSION

Single cell Isolation and characterization

Diameters (~12.5 μm) were measured for a set of cells isolated from each region with and without chloroquine treatment (Figure S-2 in Supporting Information). A One-Way ANOVA indicated that neither spatial location nor pharmacological treatment significantly altered cell size ($p = 0.24$).

HCT 116 MCTSs have a radius of approximately 500 μm. The inner 250-μm radius is a fully necrotic core region consisting of dead cells and cellular debris while the outer 250 μm consists of concentric spherical cellular layers.[4–5] In one experiment, up to 10 rounds of serial trypsinization were performed before reaching the fully necrotic core, at which point the spheroid architecture disintegrated. Assuming equal effectiveness, each trypsinization iteration removed a ~25 μm layer, corresponding to a layer two cells thick. This result is consistent with the initial report of serial trypsinization, which determined that dissociated layers of mouse mammary tumor MCTSs were 24-μm thick,[8] and with subsequent reports on the technique.[9–11]

The first three iterations of serial trypsinization isolated cells from the outer 75 μm (outer proliferative region) of the HCT 116 MCTSs, approximately six concentric layers thick. The middle region contained cells from the next three iterations of serial trypsinization, corresponding to six more concentric cellular layers at a depth of 75–150 μm. The pre-necrotic core region at a depth of 150–250 μm consisted of approximately eight concentric cellular layers. The dead cells and debris were discarded.

Three color electropherograms

A three-color electropherogram of the substrate-containing incubation medium is presented in Figure S-3 (Supporting Information). Only trace impurities were noted. Separation efficiencies exceeded 200,000 theoretical plates.

A total of 192 single cells generated signals within the linear range of our photodiodes: 33, 32, and 35 cells were analyzed from the outer, middle, and core regions of naïve HCT 116 MCTSs (respectively) and 29, 30, and 33 cells were analyzed from the outer, middle, and core regions of chloroquine-treated HCT 116 MCTSs.

Figure 2 presents the three-color electropherograms generated from a set of 29 cells isolated from the outer layer of the MCT 116 MCTS. Electropherograms generated from other portions of the MCTS and from cells treated with chloroquine are presented as Figures S-4 and S-5 (Supporting Information). In general, components are well resolved, and the electrophoretic pattern is quite consistent for each substrate.

Effect of Chloroquine on Fluorescent GSL Uptake

Cells treated with chloroquine appeared to generate much larger signals than untreated cells. Assuming that metabolism does not change the spectral property of the dye, the total fluorescence signal within a spectral channel of an electropherogram is proportional to the amount of fluorescent substrate taken up by the cell. Figure S-6 (Supporting Information) shows that chloroquine treatment significantly ($p<0.05$ to $p<0.001$) increased uptake of the substrates in the outer and middle, but not the core regions of HCT 116 MCTSs.

This increase in uptake is consistent with chloroquine's known short-term (under 2 hr) increase in uptake of exogenous species including lipids; at longer times, chloroquine can also inhibit uptake.[3242] Differences between fluorescent GSL and chloroquine transport presumably resulted in the observed spatial distribution of uptake of the fluorescent GSLs,

where chloroquine treatment significantly increased uptake only within the outer and middle regions of the HCT 116 MCTSs. The culture medium containing the fluorescent GSLs and chloroquine would be more accessible to the outer and middle regions of HCT MCTSs. If chloroquine transport to cells within the core region lags that of the fluorescent GSLs by 2 hr or more, chloroquine will not increase uptake in the core region, yet would still retain its action as a potent catabolic inhibitor.

Metabolic Cytometry of HCT 116 MCTSs

Electropherograms plotted as the mean ± one standard error of the mean are shown in Figures 3A, 3B, and 3C for the untreated cells; Figures 3D, 3E, and 3F expand the vertical axis to highlight low-level metabolites. Average electropherograms for the chloroquine-treated cells are shown in Figures 3G, 3H, and 3I; Figures 3J, 3K, and 3L present enlargements.

During the 24 hour incubation, fluorescent GSLs were taken up, transported, and metabolized in all regions of the HCT 116 MCTSs. Single cells within all regions, regardless of pharmacological treatment, showed both anabolism and catabolism of the GM3-BODIPY-FL and LacCer-BODIPY-650/665 substrates. GM1-BODIPY-TMR primarily exhibited catabolism. Occasionally, some anabolic products (likely GD1a or GD1b based on their migration time[21]) generated peaks that migrated before GM1-BODIPY-TMR, but these peaks did not appear in the majority of electropherograms and when they did appear, their heights were near the noise floor.

LacCer-BODIPY-FL, the first catabolic product of GM3-BODIPY-FL, was the most abundant BODIPY-FL labeled species observed in untreated cells, which indicates that GM3-BODIPY-FL underwent rapid catabolism. The GM1-BODIPY-TMR substrate and its catabolic product GM2-BODIPY-TMR dominated the BODIPY-TMR traces. The LacCer-BODIPY-650/665 substrate was the most abundant component within the BODIPY-650/665 traces. LacCer was the most abundant species in both the BODIPY-FL and BODIPY-650/665 channels. The accumulation of LacCer suggests that its metabolism was slower than that of the other GSL species in these HCT 116 cells.

Peak areas for each analyte were calculated and a one-way ANOVA was used to determine whether cellular localization within naïve HCT 116 MCTSs influenced the presence of specific GSL species. Asterisks located above peaks in Figures 3A, 3B, and 3C indicate a significant difference ($p<0.05$) in GSL metabolism between the three regions. All GM3-BODIPY-FL metabolites showed differential abundance as a function of location, while substrate abundance did not significantly change. The substrate GM1-BODIPY-TMR as well as its metabolites GM2-, LacCer- and GlcCer-BODIPY-TMR showed differential abundance within the MCTS architecture. Finally, the substrate LacCer-BODIPY-650/665 and its metabolites GM1-, GM2-, GlcCer- and Cer-BODIPY-650/665 exhibited differential abundance with location.

The procedure was repeated for chloroquine-treated HCT 116 MCTSs. Again, all GM3-BODIPY-FL metabolites demonstrated differential abundance while the GM3-BODIPY-FL substrate was unchanged. GM1-, GM2-, LacCer-, GlcCer-, and Cer-BODIPY-TMR showed differential abundance with cellular location, while GM3-BODIPY-TMR did not. Only the substrate LacCer-BODIPY-650/665 and its catabolic product Cer-BODIPY-650/665 showed differential abundance within chloroquine-treated HCT 116 MCTSs.

The traces in Figure 3 were recompiled to better illustrate the effect of chloroquine on GSL metabolism as a function of spatial location, Figure 4. Student's t-Tests on peak areas were used to determine whether chloroquine significantly altered GSL metabolism. With the

exception of GlcCer-BODIPY-650/665 within the middle region, chloroquine significantly altered the production of all catabolic products from all three fluorescent substrates in single cells isolated from all three spatial locations within HCT 116 MCTSs ($p < 0.05$). Nearly all of those differences were reductions in GSL abundance with the exception of LacCer-BODIPY-FL, GM2-BODIPY-TMR, and LacCer-BODIPY-650/665, which increased in abundance after chloroquine treatment.

Catabolism of GSLs mainly occurs within the lysosome, yet the lysosomal inhibitor chloroquine caused an increase in the relative abundances of a few catabolic metabolites. There are three possible reasons for this effect. First, it is possible that some GSL catabolic enzymes were more pH sensitive than others, since chloroquine dramatically increases intralysosomal pH.[31] Second, chloroquine could have targeted selected enzymes responsible for GSL catabolism, much as it targets selected lysosomal hydrolases.[32] The third possibility is kinetic, which would imply rapid catabolism of GM3-BODIPY-FL and GM1-BODIPY-TMR. If the transport and catabolism of these substrates were more rapid than the transport and pharmacological action of chloroquine, a buildup of some catabolic products in cells would be expected as the kinetics of GSL catabolism outran the kinetics of chloroquine action. When chloroquine does take effect, subsequent catabolism would be quenched.

The observed increase in the relative abundance of LacCer-BODIPY-650/665 upon chloroquine treatment again suggests that LacCer catabolism was relatively slow. GSLs initially reside in the cell membrane and rely on recycling to enter cellular compartments.[43–44] Therefore, the increase in relative abundance of LacCer-BODIPY-650/665 may be related to a decrease in intracellular trafficking of cell surface lipids produced by chloroquine.[33] Since GM3-BODIPY-FL and GM1-BODIPY-TMR were not affected in the same way, this hypothesis is unlikely unless the effects of chloroquine involve selective targeting of LacCer-BODIPY-650/665 enriched portions of the cellular membrane.

The effect of chloroquine on the relative abundance of each fluorescent GSL species is summarized in Figures S-7, S-8, and S-9 (Supporting Information). This view of GSL metabolic abundance reiterates the information shown in Figures 3 and 4, highlighting the variation in GSL metabolism as a function of both cellular location and pharmacological treatment within single cells isolated from HCT 166 MCTSs.

Quantifying Cell-to-Cell Variation in GSL Metabolism

Each cell produced a three-color electropherogram that contains information on that cell's GSL metabolism, starting from three different points in the metabolic cascade. We used principal component analysis to characterize the cell-to-cell heterogeneity in that metabolism. We first reduced dimensionality by concatenating the three-color data array into a onedimensional vector for each electropherogram as described in the experimental section.

Principal component analysis was performed on the concatenated electropherograms. Six principal components were retained as determined by a Scree plot,[45] corresponding to 91.5% of the total information content within the 192 electropherograms. A score plot of the first and second principal components is given in Figure 5A with the single cell electropherograms grouped by condition. Each point represents an entire three-color electropherogram taken from a single cell. The scatter shown in Figure 5A highlights the rich cellular diversity present in GSL metabolism.

Cells from the outer, middle, and core regions of untreated HCT 116 MCTSs tended to overlap in the score plot. Cells from the outer (•) and middle (x) regions of chloroquine-

treated MCTSs overlapped but were distinct from cells from the other conditions. This result indicated that, on average, chloroquine treatment caused the GSL metabolism of single cells within the outer and middle regions of the HCT 116 MCTSs to more closely resemble one another and differ from cells within the core region. This result is similar to a report of spheroids treated with irinotecan.[4] At 24 hours of irinotecan incubation, IMS revealed that the outer and middle regions of HCT116 spheroids showed similar mass spectral characteristics and the outer region gave a metabolically distinct small molecule profile compared to that of the central core.

In scatterplots such as Figure 5A, the data's heterogeneity can be measured as the degree of scatter in the distance between points and the center of the cluster. The Euclidean norm (*EN*) is traditionally used to calculate distance between points.

Anderson proposed a distance-based test for population homogeneity of multivariate dispersions within multivariate principal component analysis space.[46] We used this distance-based test to determine if the degree of cell-to-cell variation present in GSL metabolism was affected by location or chloroquine treatment. First, principal component analysis was performed on the concatenated single cell electropherograms. Next, the scores were grouped by condition (outer, middle, and core, with and without chloroquine). This grouping yielded a *j*-by-*k* matrix **S** where *j* represented the number of single cell electropherograms within a condition and *k* represented the number of relevant principal components. ENs were then calculated between the scores from cells in each group and the center that group

$$EN_j = \sqrt{\sum_{k=1}^{6} (S_{jk} - M_{J_k})^2} \quad \text{(Eq. 1)}$$

where M_{Jk} represented the median score for all *j* samples along a specific principal component *k*. Multivariate means (centroids), multivariate trimmed means, and multivariate spatial medians can all be used to estimate the multivariate center of a data cluster, but the multivariate spatial median is a more robust measure that makes no assumption of the underlying statistical distribution of the data.[47]

This analysis yielded six groups of distances (one for each condition investigated) indicating of the degree of heterogeneity in single cell GSL metabolism. A bar graph of these distances is shown in Figure 5B. A One-Way ANOVA was then used to test whether spatial location or chloroquine-treatment significantly altered the spread/heterogeneity of single cell electropherograms. A p value of 0.45 was obtained, indicating that the cell-to-cell variation of GSL metabolism did not change with location within the HCT 116 MCTS or with chloroquine treatment.

This result does not indicate that GSL metabolism does not vary within single cells; the single cell traces shown in Figures S-5 and S-6 (Supporting Information) as well as the score plot shown in Figure 5A clearly illustrate metabolic heterogeneity. Instead, this result indicates that neither spatial location nor chloroquine treatment significantly alter *the degree* to which single cells exhibit GSL metabolic heterogeneity.

CONCLUSIONS

We report several developments in single cell metabolic analysis. This is the first report of CE with three-color LIF detection for single cell analyses. This is the first report of the use of metabolic cytometry to analyze single cells within a biological system that mimics the development of microenvironments similar to those found in tumors. Metabolic cytometry has been used to monitor GSL metabolism in cells isolated from primary neuronal

tissue,[27–29] but the tissue was triturated into single cells *before* GSL incubation, loosing all information on the cellular position within the complex tissue. Maintaining the tissue's architecture during incubation allowed us to probe the inherent differences in the GSL metabolome as a function of location on a single cell level. We also successfully analyzed pharmacological effects of the lysosomal inhibitor and potential therapeutic chloroquine on a single cell level, which consistently resulted in decreased catabolism for all substrates and spheroid regions.

Finally, coupling principal component analysis with a distance-based heterogeneity measure allows is a simple, elegant, and powerful way to statistically quantify and compare cell-to-cell variability on a multi-faceted whole-spectrum level. Traditional measures of single cell heterogeneity in flow cytometry rely on coefficients of variation from the measurement of a few discrete parameters.[48] Here, we characterize heterogeneity based on three-color electropherograms, dramatically increasing the information content of the measurement. To our knowledge, this is the first use of such an approach to characterize cell-to-cell variation and could be readily expanded to include other measurements, including optical and mass spectrometry, surface analyses, *etc.*

Supplementary Material

Refer to Web version on PubMed Central for supplementary material.

Acknowledgments

The authors acknowledge Dr. Ole Hindsgaul and Dr. Monica Palcic for their gift of the fluorescent GSL substrates and Dr. Ronald Schnaar and Dr. Jill Prendergast for helpful discussions. Funding was provided by the 2011 Starter Grant from the Society for Analytical Chemists of Pittsburgh and The University of Notre Dame (A.B.H.) and grant R01NS061767 from the National Institutes of Health (N.J.D)

References

1. Friedrich J, Ebner R, Kunz-Schughart LA. Int. J. Radiat. Biol. 2007; 83:849–871. [PubMed: 18058370]
2. Yamada KM, Cukierman E. Cell. 2007; 130:601–610. [PubMed: 17719539]
3. Hirschhaeuser F, Menne H, Dittfeld C, West J, Mueller-Klieser W, Kunz-Schughart LA. J. Biotechnol. 2010; 148:3–15. [PubMed: 20097238]
4. Liu X, Weaver EM, Hummon AB. Anal. Chem. 2013; 85:6295–6302. [PubMed: 23724927]
5. Li H, Hummon AB. Anal. Chem. 2011; 83:8794–8801. [PubMed: 21992577]
6. Knowles HJ, Phillips RM. Anticancer Res. 2001; 21:2305–2311. [PubMed: 11724287]
7. McMahon KM, Volpato M, Chi HY, Musiwaro P, Poterlowicz K, Peng Y, et al. J. Proteome Res. 2012; 11:2863–2875. [PubMed: 22416669]
8. Freyer JP, Sutherland RM. Cancer Res. 1980; 40:3956–3965. [PubMed: 7471046]
9. McMahon KM, Volpato M, Chi HY, Musiwaro P, Poterlowicz K, Peng Y, Scally AJ, Patterson LH, Phillips RM, Sutton CW. J. Proteome Res. 2012; 11:2863–2875. [PubMed: 22416669]
10. Benita Y, Kikuchi H, Smith AD, Zhang MQ, Chung DC, Xavier RJ. Nucleic Acids Res. 2009; 37:4587–4602. [PubMed: 19491311]
11. Freyer JP, Sutherland RM. Cancer Res. 1986; 46:3513–3520. [PubMed: 3708583]
12. Cohen D, Dickerson JA, Whitmore CD, Turner EH, Palcic MM, Hindsgaul O, Dovichi NJ. Annu. Rev. Anal. Chem. 2008; 1:165–190.
13. Schnaar, RL.; Suzuki, A.; Stanley, P., editors. Essentials of Glycobiology. 2nd ed. Cold Spring Harbor (NY): 2009.
14. Piccinini M, Scandroglio F, Prioni S, Buccinna B, Loberto N, Aureli M, et al. Mol. Neurobiol. 2010; 41:314–340. [PubMed: 20127207]

15. Lavie Y, Cao HT, Volner A, Lucci A, Han TY, Geffen V, et al. J. Biol. Chem. 1997; 272:1682–1687. [PubMed: 8999846]
16. Hakomori S. Cancer Res. 1996; 56:5309–5318. [PubMed: 8968075]
17. McKibbin J, Arcolano L, Karlsson KA, Larson G, Thurin J, Brattain M. Biochim. Biophys. Acta. 1988; 958:235–246. [PubMed: 3337838]
18. Nojiri H, Manya H, Isono H, Yamana H, Nojima S. FEBS Lett. 1999; 453:140–144. [PubMed: 10403391]
19. Pahlsson P, Spitalnik SL, Spitalnik PF, Fantini J, Rakotonirainy O, Ghardashkhani S, et al. Arch. Biochem. Biophys. 2001; 396:187–198. [PubMed: 11747296]
20. Larsson EA, Olsson U, Whitmore CD, Martins R, Tettamanti G, Schnaar RL, et al. Carbohydr. Res. 2007; 342:482–489. [PubMed: 17069778]
21. Sarver SA, Keithley RB, Essaka DC, Tanaka H, Yoshimura Y, Palcic MM, et al. J. Chromatogr. A. 2012; 1229:268–273. [PubMed: 22321948]
22. Keithley RB, Rosenthal AS, Essaka DC, Tanaka H, Yoshimura Y, Palcic MM, et al. Analyst. 2013; 138:164–170. [PubMed: 23154386]
23. Dovichi NJ, Hu S. Curr. Opin. Chem. Biol. 2003; 7:603–608. [PubMed: 14580565]
24. Whitmore CD, Hindsgaul O, Palcic MM, Schnaar RL, Dovichi NJ. Anal. Chem. 2007; 79:5139–5142. [PubMed: 17567107]
25. Keithley RB, Metzinger MP, Rosado AM, Dovichi NJ. Talanta. 2013; 111:206–214. [PubMed: 23622546]
26. Krylov SN, Zhang Z, Chan NW, Arriaga E, Palcic MM, Dovichi NJ. Cytometry. 1999; 37:14–20. [PubMed: 10451502]
27. Krylov SN, Starke DA, Arriaga EA, Zhang ZR, Chan NWC, Palcic MM, et al. Anal. Chem. 2000; 72:872–877. [PubMed: 10701276]
28. Essaka DC, Prendergast J, Keithley RB, Hindsgaul O, Palcic MM, Schnaar RL, et al. Neurochem. Res. 2012; 37:1308–1314. [PubMed: 22407243]
29. Essaka DC, Prendergast J, Keithley RB, Palcic MM, Hindsgaul O, Schnaar RL, et al. Anal. Chem. 2012; 84:2799–2804. [PubMed: 22400492]
30. Loeb F, Clark WM, Coatney GR, Coggeshall LT, Dieuaide FR, Dochez AR, et al. J. Am. Med. Assoc. 1946; 130:1069–1070. [PubMed: 21019115]
31. Ohkuma S, Poole B. Proc. Natl. Acad. Sci. U.S.A. 1978; 75:3327–3331. [PubMed: 28524]
32. Dijkstra J, Van Galen M, Scherphof GL. Biochim. Biophys. Acta. 1984; 804:58–67. [PubMed: 6722184]
33. Schneider YJ, Trouet A. Eur. J. Biochem. 1981; 118:33–38. [PubMed: 6793366]
34. Yuyama K, Yamamoto N, Yanagisawa K. FEBS Lett. 2006; 580:6972–6976. [PubMed: 17161396]
35. Zhou ST, Zhao LJ, Kuang MC, Zhang BJ, Liang Z, Yi T, Wei YQ, Zhao X. Cancer Lett. 2012; 323:115–127. [PubMed: 22542808]
36. Kimura T, Takabatake Y, Takahashi A, Isaka Y. Cancer Res. 2013; 73:3–7. [PubMed: 23288916]
37. Pagano RE, Watanabe R, Wheatley C, Dominguez M. Method. Enzymol. 2000; 312:523–534.
38. Sobhani K, Michels DA, Dovichi NJ. Appl. Spectrosc. 2007; 61:777–779. [PubMed: 17697473]
39. Turner EH, Lauterbach K, Pugsley HR, Palmer VR, Dovichi NJ. Anal. Chem. 2007; 79:778–581. [PubMed: 17222051]
40. Whitmore CD, Essaka D, Dovichi NJ. Talanta. 2009; 80:744–748. [PubMed: 19836546]
41. Hendler RW, Shrager RI. J. Biochem. Bioph. Meth. 1994; 28:1–33.
42. Dijkstra J, van Galen M, Regts D, Scherphof G. Eur. J. Biochem. 1985; 148:391–397. [PubMed: 3987696]
43. Merrill AH Jr. Chem. Rev. 2011; 111:6387–6422. [PubMed: 21942574]
44. Chen CS, Martin OC, Pagano RE. Biophys. J. 1997; 72:37–50. [PubMed: 8994591]
45. Jolliffe, IT. Principal Component Analysis. New York, NY: Springer Science; 2002. p. 111-133.
46. Anderson MJ. Biometrics. 2006; 62:245–253. [PubMed: 16542252]
47. Brown MB, Forsythe AB. J. Am. Stat. Assoc. 1974; 69:364–367.

48. Shapiro, HM. Practical Flow Cytometry. Hoboken, NJ: John Wiley & Sons, Inc.; 2003. p. 225-256.

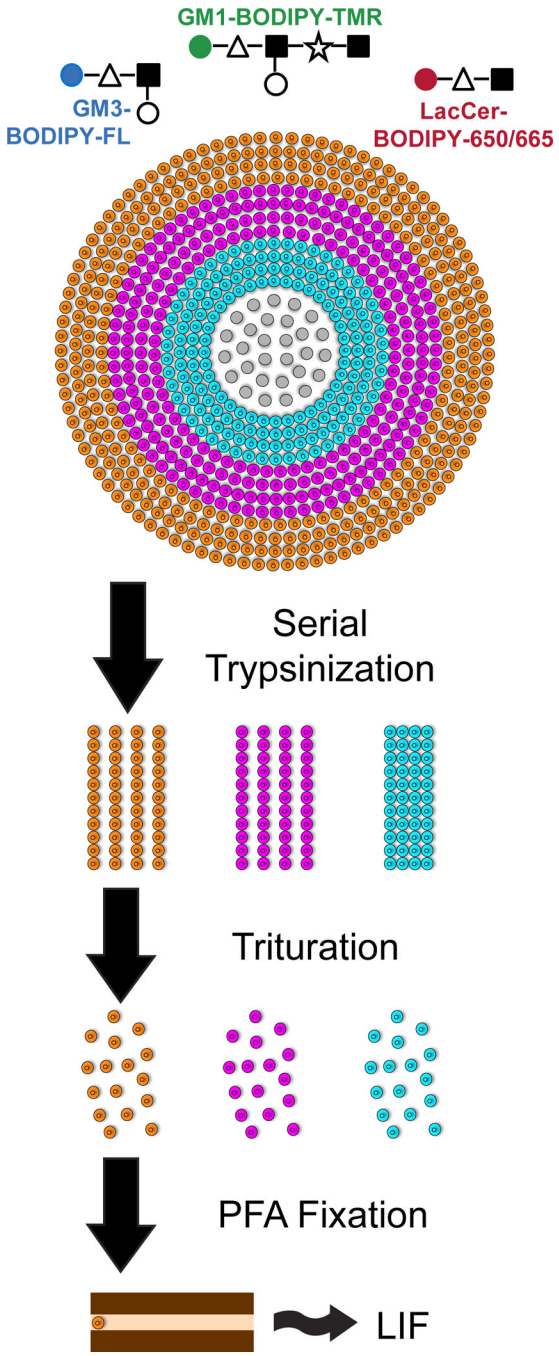

Figure 1.

Experimental overview. HCT 116 MCTSs were simultaneously incubated with GM3-BODIPY-FL, GM1-BODIPY-TMR, and LacCer-BODIPY-650/665. After 24 hours, the spheroids underwent serial trypsinization, yielding sheets of cells from the outer (orange), middle (magenta), and core (cyan) regions. Dead cells and cellular debris are contained within the center (grey); this material was discarded. These cellular sheets underwent trituration to isolate individual cells and the cells were then fixed with paraformaldehyde (PFA). After fixation, cells were analyzed with CE-LIF.

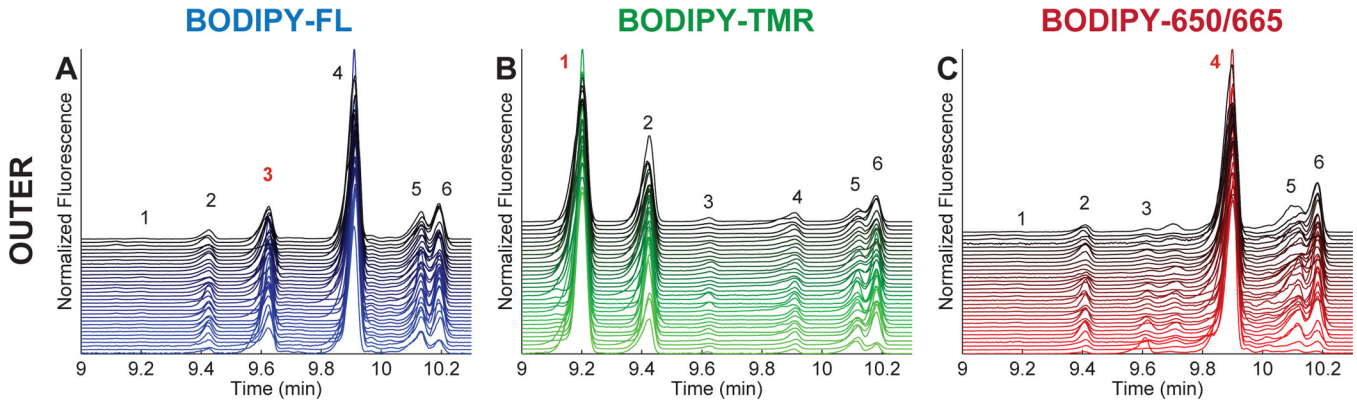

Figure 2.

Electropherograms from single cells of HCT 116 MCTSs. A, B, and C show GM3-BODIPY-FL, GM1-BODIPY-TMR, and LacCer-BODIPY-650/665 metabolism (respectively) in single cells contained within the outer region of HCT 116 MCTSs. Numbers indicate the metabolic product (1-GM1, 2-GM2, 3-GM3, 4-LacCer, 5-GlcCer, and 6-Cer). Red numbers indicate the fluorescent substrate for each channel.

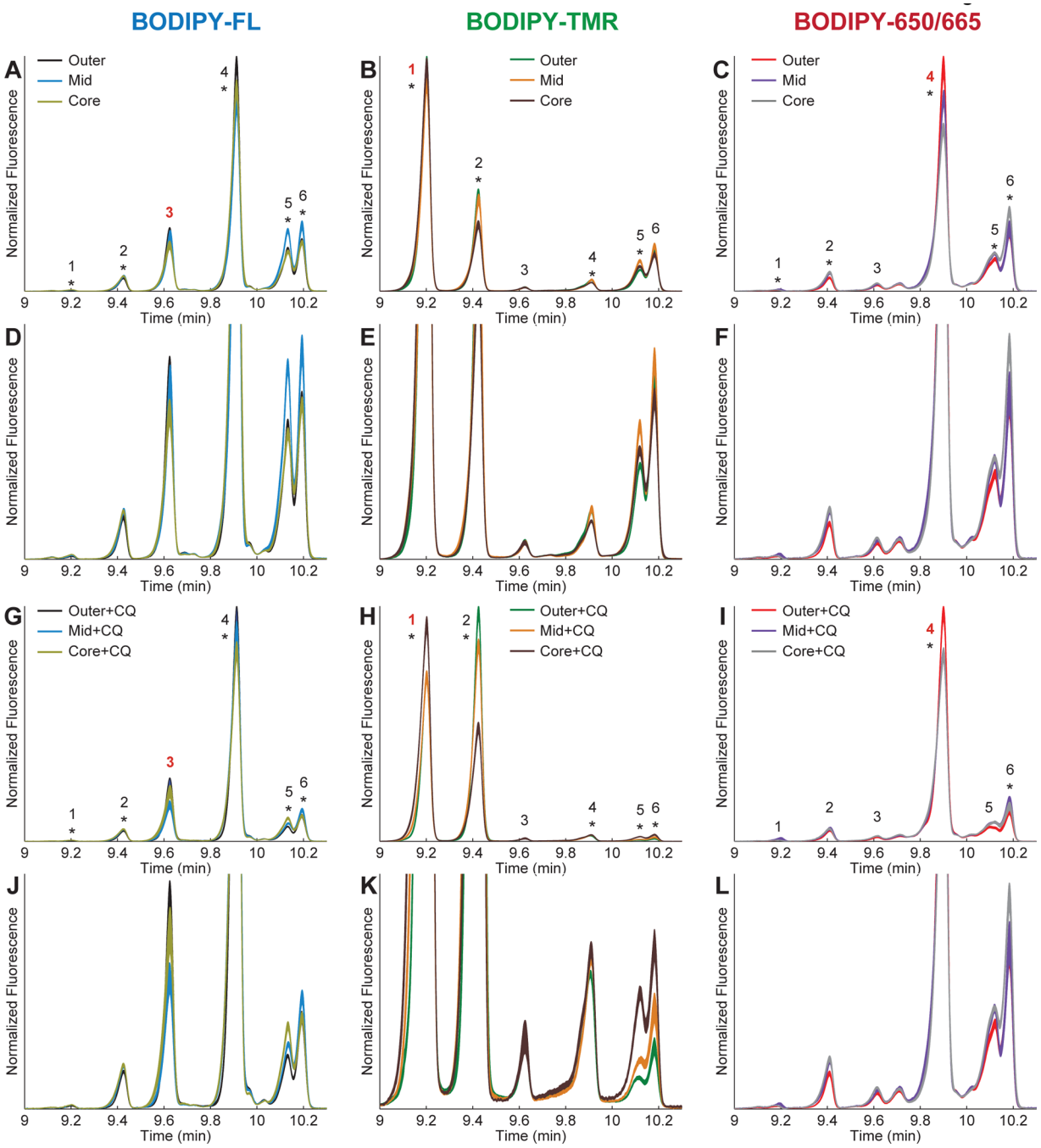

Figure 3.

Average multicolor metabolic cytometry electropherograms, normalized to unit area, for each region within the spheroids. The line width encompasses ± standard error of the mean for all cells in each location and pharmacological condition. **A, B,** and **C** compare GM3-BODIPY-FL, GM1-BODIPY-TMR, and LacCer-BODIPY-650/665 metabolism (respectively) by location in HCT 116 MCTS single cells. **D, E,** and **F** present enlargements of the Y-axis of **A, B,** and **C** (respectively). **G, H,** and **I** compare by location in chloroquine (CQ)-treated MCTS. **J, K,** and **L** present enlargements of the Y-axis of **G, H,** and **I** (respectively). Numbers indicate the metabolic product (1-GM1, 2-GM2, 3-GM3, 4-LacCer,

5-GlcCer, and 6-Cer). Red numbers indicate the fluorescent substrate in each channel. An asterisk indicates a significant difference ($p < 0.05$) in peak area using a One-Way ANOVA as described in the text.

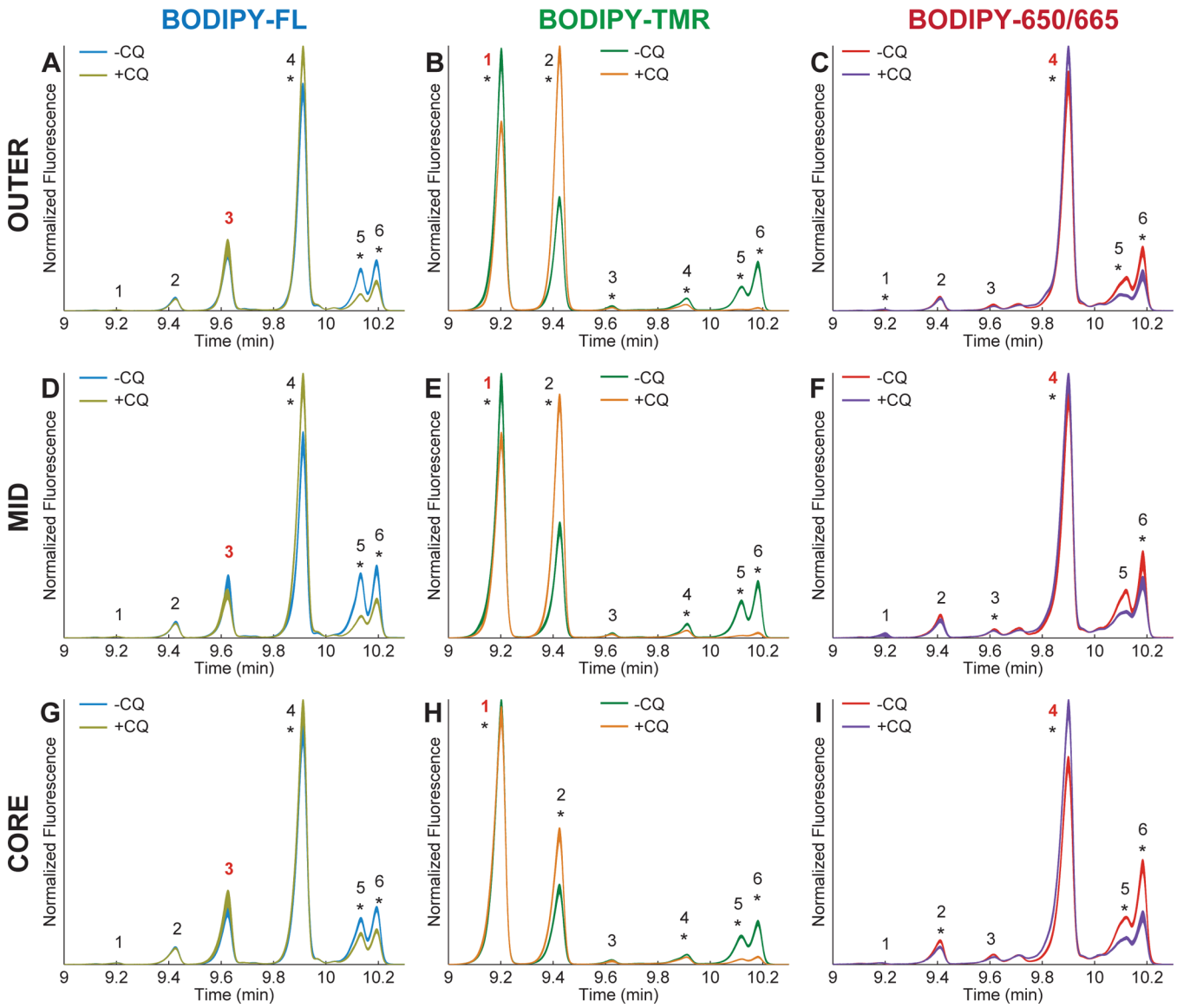

Figure 4.

Effect of chloroquine treatment on fluorescent GSL metabolism by region. The data in Figure 3 are recompiled to illustrate the effect of chloroquine (CQ) in different regions. Each colored trace is shaded to encompass ± standard error of the mean for all cells in a specified location and pharmacological condition. **A, B,** and **C** show the effect of CQ on GM3-BODIPY-FL, GM1-BODIPY-TMR, and LacCer-BODIPY-650/665 metabolism (respectively) in single cells from HCT 116 MCTSs located within the outer region. **D, E,** and **F** show the effect of CQ on GM3-BODIPY-FL, GM1-BODIPY-TMR, and LacCer-BODIPY-650/665 metabolism (respectively) within the middle region. **G, H,** and **I** show the effect of CQ on GM3-BODIPY-FL, GM1-BODIPY-TMR, and LacCer-BODIPY-650/665 metabolism (respectively) within the core region. Numerical indices are the same as those depicted in Figure 3. An asterisk indicates a significant difference ($p < 0.05$) in peak area using a Student's t-test as described in the text.

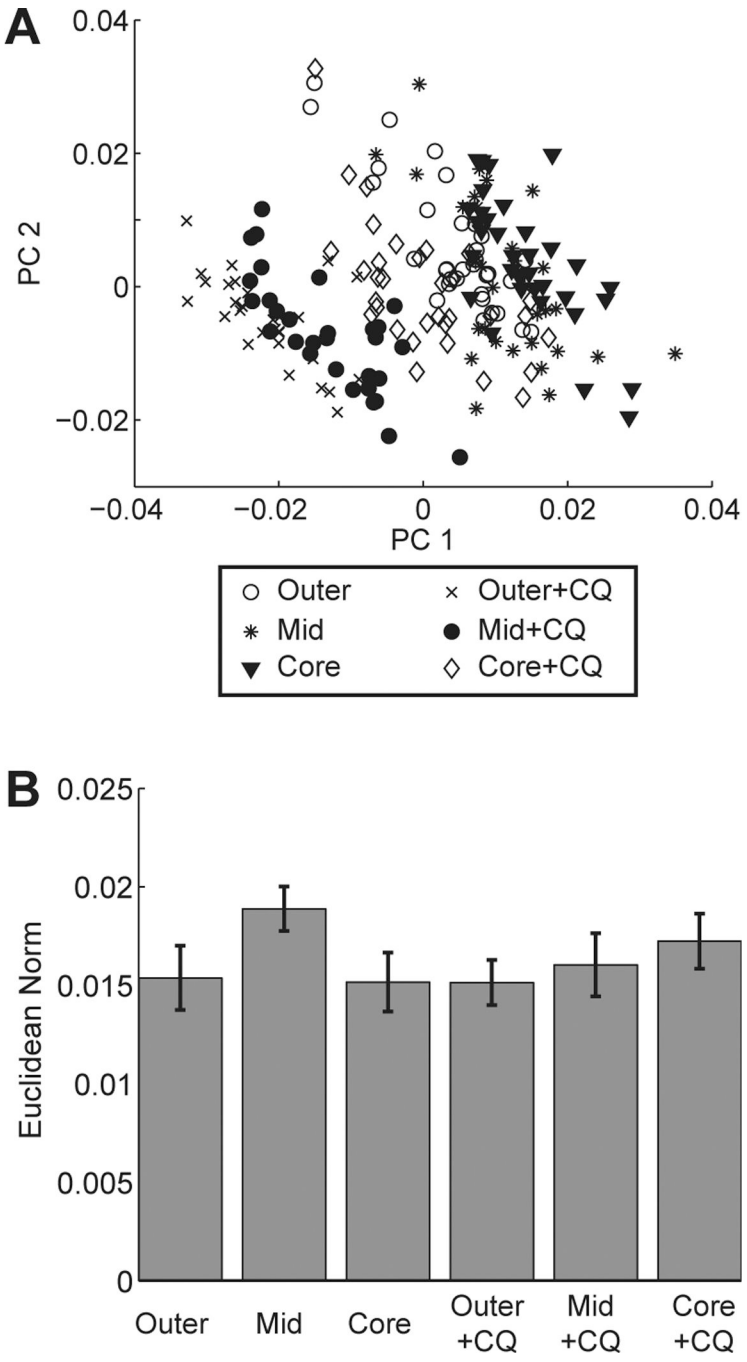

Figure 5.

Principal component analysis of multicolor single cell electropherograms. **A.** PC1 versus PC2 score plot of the concatenated multicolor electropherograms for each cell in each condition. **B.** Plot of the Euclidiean Norm of PCA scores between each point within a specified cluster and the multivariate spatial median for all points within the specified cluster. Error bars are ± one standard error of the mean.